sciendo

Geologos 29, 1 (2023): 33–49
https://doi.org/10.14746/logos.2023.29.1.03

GEOLOGOS

Palaeoenvironmental and palaeoclimatic inferences based on X-ray computer tomography: a case study of alkaline lake deposits in Hungary

Nour N. Alzoubi*, Sandor Gulyas, Janos Geiger

The University of Szeged, Department of Geology and Palaeontology, 2-6 Egyetem u., 6722 Szeged, Hungary
* corresponding author; e-mail: nouralzoubi@geo.u-szeged.hu

Abstract

Widely distributed freshwater carbonate sediments, i.e., limestone, dolomitic limestone and dolomite, developed in inter-dune alkaline ponds of the Danube-Tisza Interfluve in the centre of the Carpathian Basin during the Holocene. The key parameters that determine the formation of any given type of carbonate mineral (calcite, dolomite) are temperature, evaporation rate, pH and ion concentrations, in addition to CO_2 absorption by aquatic plants. CT analysis is capable of recording small-scale density variations attributable to compositional differences of sedimentary rocks. As the type and proportion of rock-forming minerals and other components is an artifact of past environmental and climatic conditions, CT values may act as potential palaeoenvironmental proxies. The present study compares variations in rock-forming components obtained for freshwater carbonates utilizing the CT method with already available geochemical and palaeoecological proxy data. Variations in molluscan ecology and isotope geochemistry, sedimentation times and CT-based rock density values all indicate the relevance of millennial-scale, climate-driven changes in carbonate formation. As previously observed, the emergence of colder conditions in the North Atlantic, which resulted in increased cyclonic activity and heavier rainfall in western Europe and the Danube watershed area between 10.3 and 9.3 kyr cal BP, resulted in the emergence of humid conditions favouring a rise in the groundwater table at our site and precipitation of calcite from pore waters as opposed to high-magnesium calcite. This is clearly reflected in a negative shift in CT density values in our dated rock samples.

Keywords: freshwater carbonate, CT analysis, statistical properties, palaeoenvironment, Holocene

1. Introduction

The area of the Danube-Tisza Interfluve (DTI), located in the heart of Hungary between the rivers Danube and Tisza, is covered by wind-blown sand and loess deposits. These sediments contain around 10% carbonate; they were shaped into dunes in a NW–SE direction by dominant north-westerly winds during the late Pleistocene and early Holocene (Mihältz, 1947, 1953; Molnár, 1976, 1988; Kercsmár, 2015). The interdune areas are occupied by alkaline lakes over the entire interfluve area complemented by a few lakes that emerged because of antecedent river regulations in the 19th century. The main source of water is groundwater which contains calcium and magnesium as well as surface runoff (Molnár, 1976; Molnár & Szónoky, 1976; Molnár et al., 1995).

High-magnesium calcite precipitates seasonally from the water based on climatic conditions and associated volume, geochemistry (pH, the concentration of dissolved elements) of the lake and pore waters, as well as fluctuations of the groundwater table. The DTI groundwater has a fairly high total dissolved solid (TDS) content; 500–2000 mg/l on average; occasionally > 5,000 mg/l. Strong evaporation affects the water level of the lakes due to high summer temperatures and little rainfall. The

TDS of lake water rises to values between 8,000 and 70,000 mg/l, as the lost water is replenished from the groundwater, making these ponds very saline and highly alkaline, with a pH ranging from 9 to 11, due to calcium, magnesium and hydro-carbonate ions (Molnár & Botz, 1996). Seasonally, towards the end of the summer, groundwater levels drop to 3–8 m below the surface, and many of the lakes dry up (Molnár & Szónoky, 1976; Molnár, 1991; Molnár et al., 1995). The ratio of Mg/Ca in the lake and pore fluids determines the precipitation of primary carbonates (calcite, high-Mg calcite, aragonite, hydrous Mg carbonate) and secondary carbonates (proto-dolomite, dolomite, huntite, magnesite). Secondary carbonates and high-Mg calcite are found in lakes when the stated ratio exceeds 7, the overall salinity of the water is high, and the salinity fluctuates greatly during the year. During periods when pore waters are exceptionally rich in Mg, proto-dolomite occurs in the mud accumulating on the lakebed through the transformation of Mg-bearing calcite (Müller et al., 1972; Gaines, 1977; Müller & Wagner, 1978; Tullner & Cserny, 2003; Chen et al., 2017; Fang & Xu, 2019).

Rainfall during the autumn supplies freshwater to the DTI alkaline lakes, thereby decreasing Na and K concentrations and increasing the Mg/Ca ratio to 7–12 creating favourable conditions for precipitation of high-magnesium calcite. The Mg/Ca ratio in the residual pore fluids rises even more, causing high-magnesium calcite to undergo early diagenetic transformation into proto-dolomite and dolomite since the CO_3/Ca ratio exceeds 1. Seasonal migration of pore water saturates the matrix and fills the pores with minerals precipitating from the residual solution (calcite, limonite), changing the carbonate mud into solid rock where the lacustrine phase of carbonate precipitation had ended (Bender et al., 1975; Molnár, 1980, 1991).

Thus, two types of carbonate are present in the region: the lower part (60–110 cm) is solid carbonate rock (dolomitic limestone) corresponding to lacustrine deposits which have undergone diagenesis, and in the upper part (30–60 cm) there is unlithified recent carbonate mud (Mihältz & Faragó, 1946; Mihältz, 1947, 1953; Mucsi, 1963; Molnár, 1970; Jenei et al., 2007; Sümegi et al., 2015; Sümegi & Náfrádi, 2015).

The composition of sedimentary rocks, i.e., the distribution of principal rock-forming components (RFCs), expresses their formation and diagenetic history. To assess the nature of these processes and the resulting spatial heterogeneity, quantitative information on RFC distribution at both macro- and micro-scales is required (Alzoubi et al., 2022).

X-ray computed tomography is a non-destructive inspection technology that produces cross-sectional tomographic images by measuring penetrating radiation intensity changes throughout various routes of a material. Such changes are linked to density variations attributable to differing chemical, physical or biological characteristics of the material under study (Maurício et al., 2017). The original application of CT was for medical purposes (Kenter, 1989), but it is now frequently employed in other fields, including archaeology, palaeontology, sedimentology and structural geology (Duliu, 1999; Ketcham & Carlson, 2001; Földes et al., 2004; Cnudde et al., 2006; Markussen et al., 2019). Post- or syndiagenetic sedimentary formations present in clastic rocks are also easily identified visually on CT images (Wilding et al., 2005). However, CT techniques were applied to heterogeneous carbonate to show the potential and limitations of CT (Hicks et al., 1994), and compare the standard mass balance equation and concentration with a CT (Fourar et al., 2005). When compared to three-dimensional methods, two-dimensional digital image analysis (2D DIA) allows the processing of any core cutting and needs little data manipulation and computing (Oliveira et al., 2020).

Apart from visual evaluation, the most essential characteristic of CT analysis are the data behind it, which contain quantitative information on density variations evident between rock-forming textural components in the material. Computer tomography analysis supplies us with quantitative data in 3D at both the scale of the entire sample and a resolution specified by voxel dimensions at micro-scale. The density of RFCs corresponds with quantitative data reported in Hounsfield units (HU) (Bhattacharyya, 2016). As a result, its statistical features capture information on their heterogeneity. In a previous study, Alzoubi et al. (2022) successfully applied such techniques to segment freshwater carbonate samples deriving from the site of Csólyospálos in the DTI into its rock-forming components (RFCs). In that work, the authors managed to estimate the proportions of the major rock-forming components, separating them into three major groups: matrix, pores and cement material. The former two carry information on the depositional history, while the last-named refers to rock diagenesis. The creation of carbonate cement infilling the pores is also a subsequent step of rock formation, thus again yielding information on the diagenetic history. The percentages of the RFCs for the samples were presented as a whole and made comparisons possible with percentage distributions estimated using thin sections. While the former was based on val-

ues inferred for the entire sample, the latter used thin sections taken only from selected parts of the sample. The data available per CT slice (Alzoubi et al., 2022) allows for the investigation of vertical and horizontal compositional changes at a much smaller scale, i.e., that of voxels. In this way minor scale changes, reflecting shifts in the depositional environment, can be tackled. Information on the textural characteristics, geochemical composition, isotope geochemistry and molluscan-based palaeoecology of carbonates from the Csólyospálos site are readily available, although at a much lower resolution (Mucsi, 1963; Molnár, 1970, 1980, 1991; Molnár & Szónoky, 1976; Molnár et al., 1995). This allows us to make a visual comparison with our high-resolution compositional data deriving from CT analysis of the samples. The present paper aims to test the applicability of CT-derived data for palaeoenvironmental reconstruction, as well as to capture and describe the vertical heterogeneity of RFCs in selected carbonate samples from the Csólyospálos site using the logic from the previous study by Alzoubi et al. (2022). This time estimations of RFCs are presented per CT slice allowing to tackle minor changes in environmental conditions. A comparison of small-scale trends (possibly centennial) with major trends (multimillennial-scale) seen in geochemical and palaeoecological records from the site enables us to refine the evolutionary history of the lacustrine sequence. In addition, periods dominated by different types of carbonate mineral precipitation may also be captured.

2. Study site

The Danube-Tisza Interfluve (DTI) is a 180-km-long and 120-km-wide, wind-blown sand and loess-covered ridge, 100–150 m a.s.l. between the rivers Danube and Tisza in central Hungary (Fig. 1A). To the west, the region is bounded by the Danube River valley tectonic depression, which is located at a height of 90–100 m a.s.l. The area's eastern limit is formed by a 10–15 km-wide valley of the Tisza River 80 m a.s.l. The DTI's bedrock created of alternating loess and wind-blown sand strata that reflect reworked Danube River deposits.

The sands were organised into a sequence of dunes with a NW to SE direction by prevailing winds throughout the late Pleistocene and Holocene. The interdune depressions are filled by a range of soda lakes, which obtain their water mostly from groundwater moving from the Danube valley to that of the Tisza River in the east. These lakes are characterised by freshwater carbonate formation (Fig.1D, F) (Molnár & Szónoky, 1976; Molnár et al., 1976).

Our study site at Csólyospálos, located on the south-eastern edge of the Danube-Tisza Interfluve (Fig. 1B), is one of these interdune lacustrine systems in which carbonate formation began around 11,500 years ago and ended around 3,500 years ago (Jenei et al., 2007; Sümegi et al., 2015; Sümegi & Náfrádi, 2015). The outcrop is located around 2 kilometres northeast of the settlement of Csólyospálos at an elevation of 92 m a.s.l. A geological section constructed in the centre of an upper Pleistocene interdune depression exposes a *c*. 1-m-thick carbonate succession covered by upper Holocene black earth soil. A Holocene dune borders the former pond in the southeast (Fig. 1C).

The carbonate series that covers the bedrock of upper Pleistocene wind-blown sand is divided into two parts: a lower lithified and a higher non-lithified. The series was subdivided into five members (Cs-1, Cs-2, Cs-3, Cs-4 and Cs-5) on the basis of its observed lithological properties (Molnár, 1970) (Fig. 1E). Cs-5 corresponds to the modern soil and as such is beyond the scope of the present analysis.

3. Methodology

3.1. Sampling

Samples in the present study correspond to the ones collected and analysed by Mucsi (1963) and housed in the sedimentary rock collection of the Department of Geology and Palaeontology, University of Szeged. All samples were originally cut in half with their surfaces polished. CT measurements were done on four samples representing all members of the Csólyospálos carbonate sequence (Cs-1, Cs-2, Cs-3 and Cs-4). Members Cs-1 and Cs-2 are represented by a single sample (sample I) taken a depth of between 65 to 90 cm in the section. Member Cs-3 is represented by two adjacent samples (samples II and III) from a depth of 65–60 cm, while member Cs-4 is represented by a single sample (sample IV) from a depth of 55–25 cm (Fig. 1E).

3.2. Computer tomography

CT scans were run for these four samples using a Siemens Emotion 6 medical scanner at the Department of Radiology, University of Pécs, Hungary. The CT scanner runs at 140 kVp, with a current of 189 mAs and a 1.5-second exposure duration. The

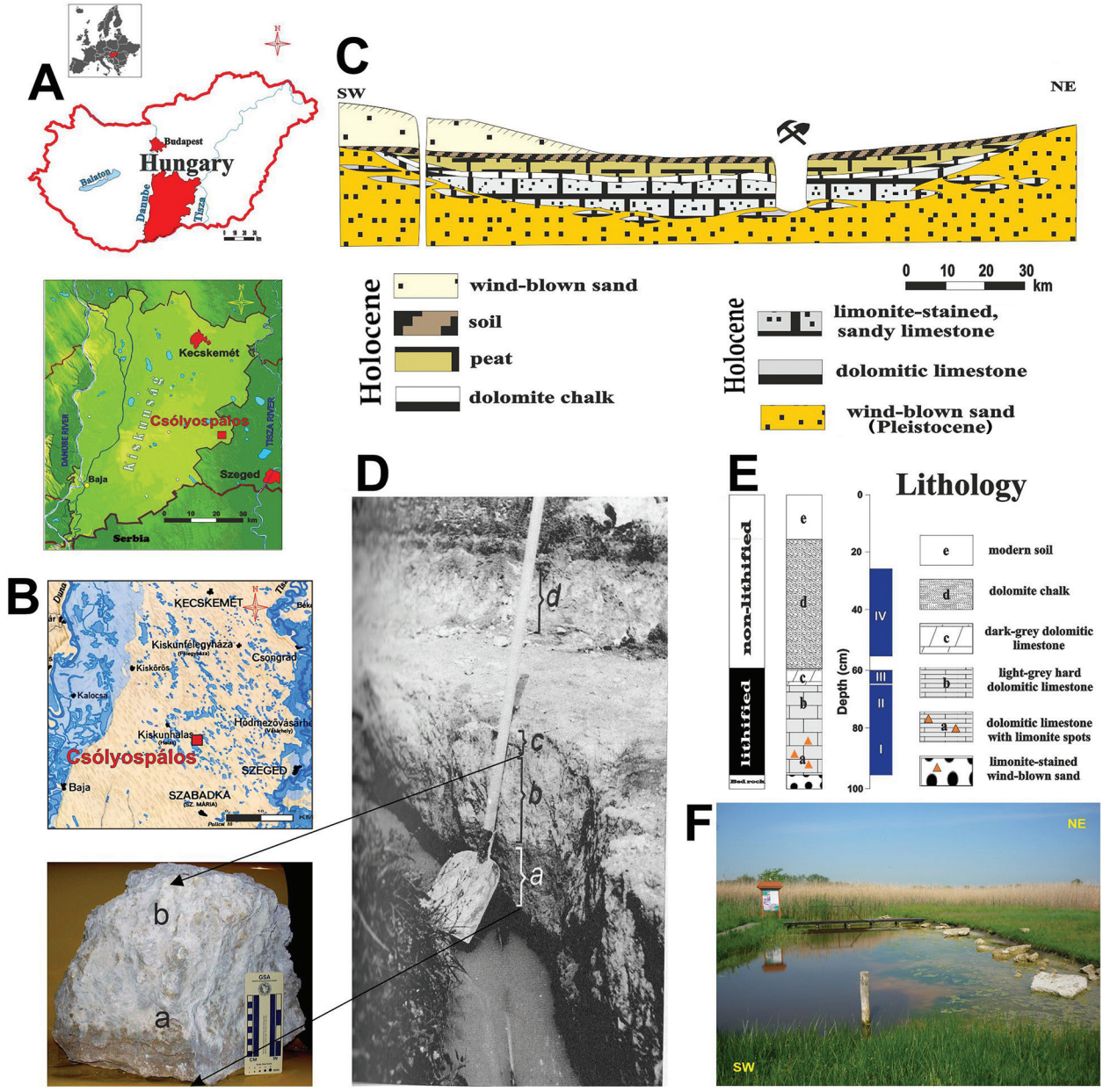

Fig. 1. Location and stratigraphy of the carbonate sequence studied near Csólyospálos. **A –** Location; **B –** Hydrography of the area, prior to the late 19th century; **C –** Geological cross-section of the site; **D –** Lithology of the site; **E –** Schematic log of the outcrop with position of samples under study marked; **F –** View of outcrop (adopted from Alzoubi et al., 2022).

slice thickness was 1.5 mm, and the lateral resolution 0.23 mm x 0.23 mm.

3.3. Workflow of analysis

The major aim of our work was to reveal small-scale vertical proportional variations in rock-forming components (RFCs) that record sedimentary environmental changes and to find correspondences with palaeoclimatic and palaeohydrological changes inferred from results of geochemical studies by Molnár & Botz (1996) and palaeoecological investigations done by Mucsi (1963). X-ray computer tomography was done to gain quantitative data based on density differences of RFCs expressed by Hounsfield unit values (HU) (Fig. 2). The CT images were exported as Digital Imaging and Communications in Medicine DICOM image and a 3D volume rendering software (Voxler 4.0) was used for visualisation, filtering and data extraction. As scanning artifacts, such as beam hardening, can

cause the CT value of a single material to change in different parts of an image, the dataset was filtered by removing the outer part of the image creating a centrally positioned CT brick (subset) smaller in volume than the original sample. Data extracted from this CT brick were used in further statistical analysis. Distribution types were visually assessed using histograms and boxplots. As our samples are assumed to represent a pool of normally distributed populations corresponding to the rock-forming components, the maximum-likelihood method of mixture analysis was adopted to recover and estimate the parameters of two or more univariate normal distributions (Mean, STD) in PAST 4.06. This method is based on the end member (EM) algorithm of Dempster et al. (1977). To determine if the number of groups chosen is appropriate and to avoid overfitting, the Akaike Information Criterion AIC (Akaike, 1974; Hammer et al., 2001) is calculated. Each data point was assigned to one of the groups using a maximum likelihood approach. The statistical parameters gained for each subpopulation were used to set HU value intervals. Using the gained parameters of the mean ± 1 and 2 STD, the recovered subpopulations were visualised, and their lithological meaning assessed. HU intervals set for each meaningful subpopulation using the referred statistical parameters can be regarded to describe rock-forming components present in the samples quantitatively.

Alzoubi et al. (2022) presented the results of RFCs defined via detailed statistical analysis of CT-scanned samples. Thus, here we just wish to show the main logic of the work by example of sample I. Five main components (A to D), presented in Figure 2, display the results of the mixture analysis of sample I (Cs-1 and Cs-2). These represent the empty pores (A), partially or almost filled pores (B), the dominantly calcitic limestone (C1), the high magnesium calcite (HMC) bearing matrix (C2) and limonite-saturated HMC and dolomitic matrix (D). As there is an overlap between these five major components a total of eight sub-components is notable: 1. empty pores, 2. partially filled pores (pores with less than 20% infill), 3. semi-filled pores (pores of ~50% filled), 4. filled pores by around (80–100% filled), 5. calcitic matrix, 6. high-magnesium calcitic (HMC)-dolomitic matrix, 7. high-magnesium calcitic (HMC)-dolomitic matrix with a minor amount of Fe^{2+} and Mn^{2+} precipitate, and 8. limonite-saturated HMC-dolomitic matrix. In the present work, HU intervals of the five major RFCs were used and percentages of RFCs were calculated for each CT slice sequentially using a script in Golden Soft-

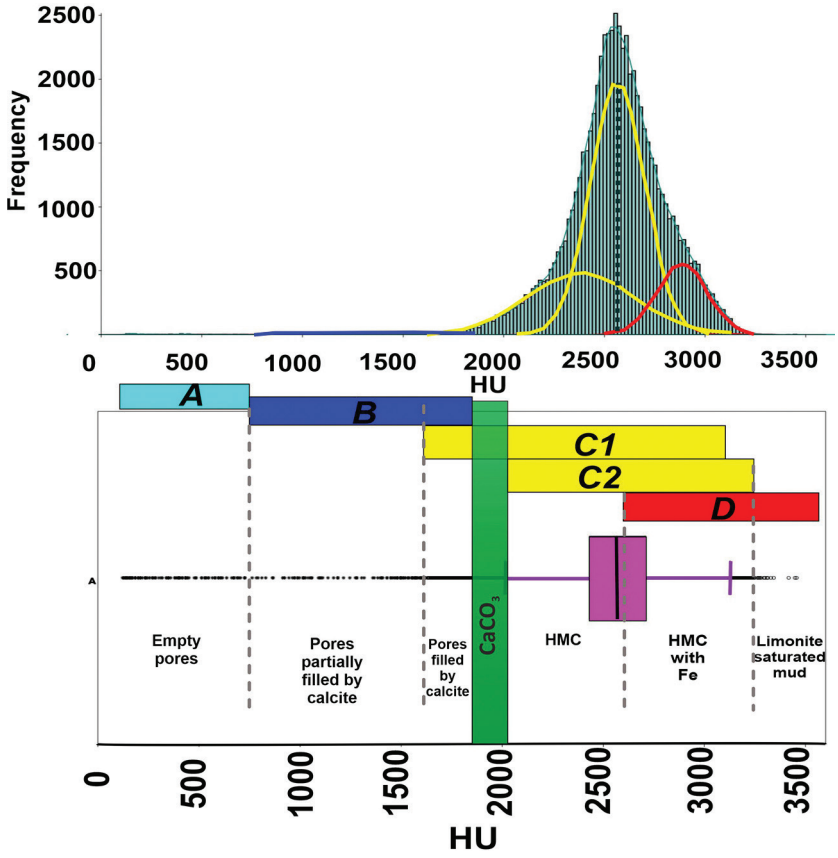

Fig. 2. Results of mixture analysis for sample I with explanation of subcomponents based on HU and RFCs (adopted from Alzoubi et al., 2022). Abbreviations: Ca – calcium, HMC – high magnesium calcite, Fe – iron.

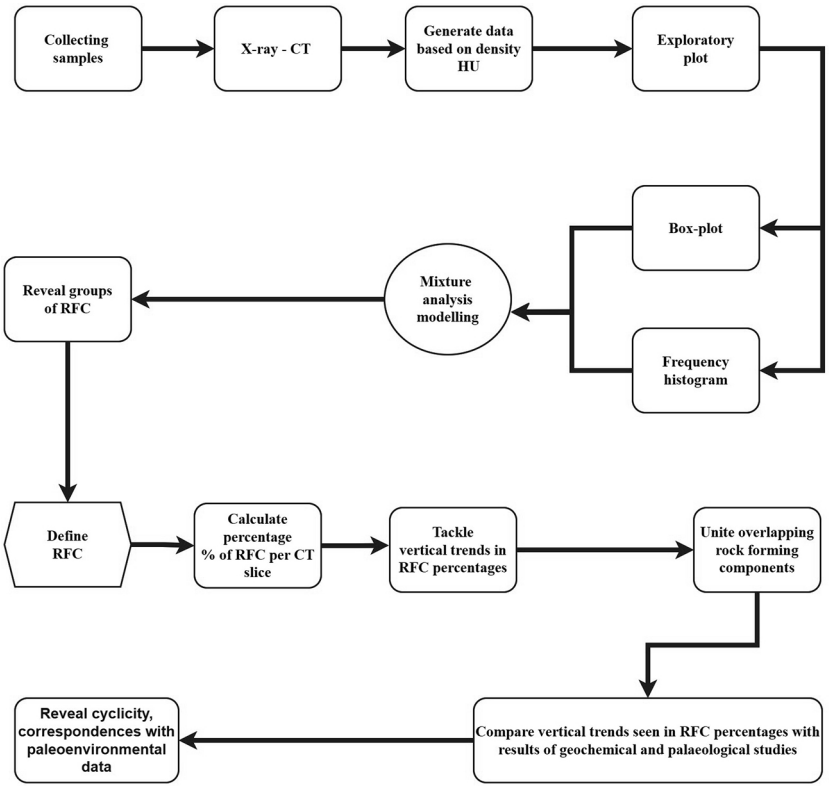

Fig. 3. The workflow applied in the present study.

ware Scripter. Major and small-scale vertical trend changes in RFC percentages of our samples were compared with geochemical data of Molnár & Botz (1996) and palaeoecological data of Mucsi (1963), supplying information on palaeohydrological and palaeoclimatological changes (Fig. 3).

3.4. Age depth modelling and sedimentation time

Radiocarbon data presented by Jenei et al. (2007), Sümegi et al. (2015) and Sümegi & Náfrádi (2015) were used to construct age-depth models. Bayesian modelling was performed using the software package RBacon (Blaauw et al., 2018). All input data were provided as ^{14}C yr BP and the model used the Northern Hemisphere IntCal20 calibration curve (Reimer et al., 2020) to convert conventional radiocarbon ages to calendar ages expressed as cal BP. Age modelling was run to achieve a 5-cm final resolution. All data and figures are presented in calendar ages expressed as cal BP. Sedimentation times (years/cm) were estimated by Markov chain Monte Carlo (MCMC) iterations using the accrate.depth.ghost and accrate.age.ghost functions of RBacon. This function allows us to capture variability in accumulation rates and assigned varying uncertainties with depth in contrast to the traditionally applied equation based on mean model ages of consecutive depths and depth intervals.

4. Results and interpretation

4.1. Members Cs-1 and Cs-2

The graphs in Figure 4 depict the vertical variation of identified RFCs for sample I (Cs-1 and Cs-2). The vertical proportion of group A - corresponding to empty pores – is relatively constant with values ranging mostly between 0 and 0.05% with some minor peaks of 0.15 and 0.2%. These deviations can be attributed to the presence of large pores in the slices also seen in Figure 5.

In group B, corresponding to the partially calcite-filled pores, there is a gradual decrease from 1.6 to 0.4% between *c.* 90 and 82 cm, followed by a pronounced increase to plateau values between 0.8 and 1.2% in general with some minor peaks of 1.6%. This plateau corresponds to the middle part of the sample after which another significant drop to 0.6–0.4% is noted in the topmost part.

The percentage of the dominantly calcitic matrix (C1) is low in the bottom and top part of the sample with values around 40–45%. Higher values of 65–75% form a plateau in the middle part of the sample

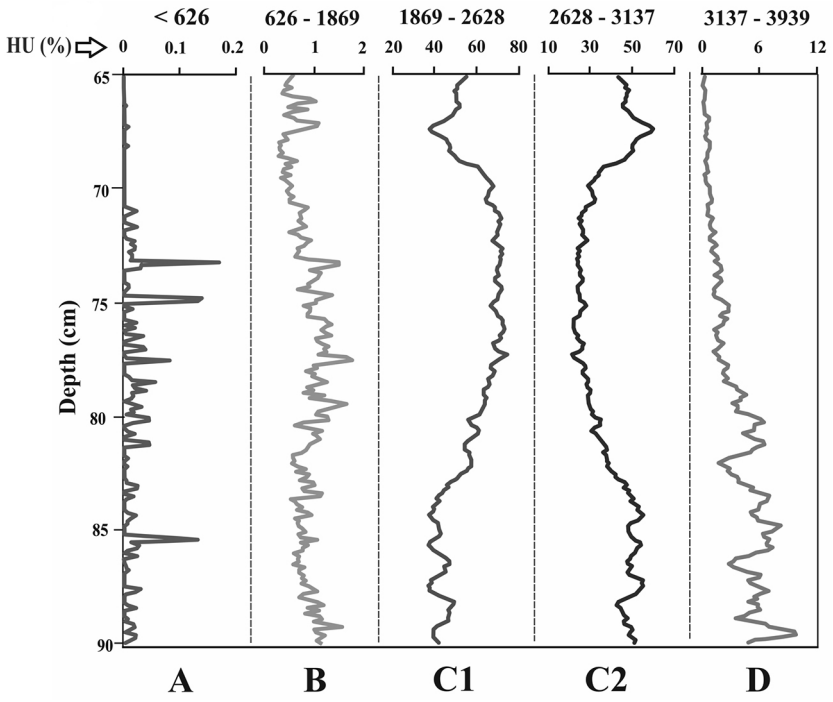

Fig. 4. Vertical changes in the proportion of identified rock-forming components (RFC) for members Cs-1 and Cs-2. A – empty pores, B – partially filled pores, C1 – low-density, predominantly calcitic matrix, C2 – high-density, predominantly dolomitic matrix, D – highest-density, limonite-saturated dolomitic matrix. Note numbers at the top mark the HU intervals of the corresponding RFCs.

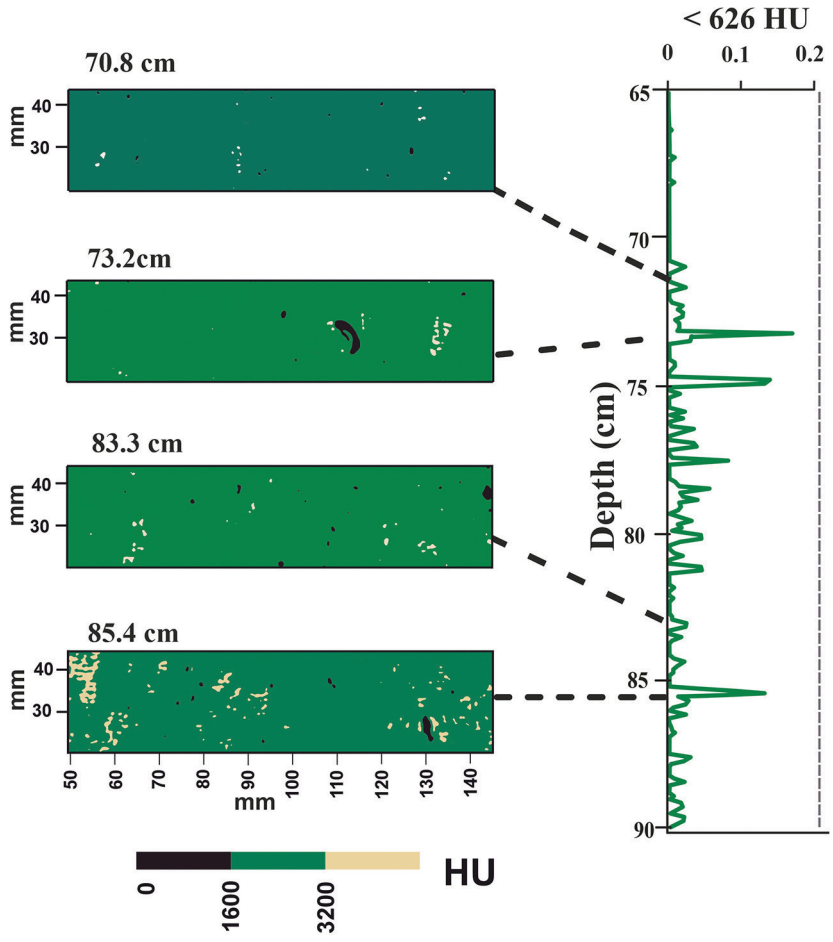

Fig. 5. Selected horizontal slices of sample I displaying the presence of large empty pores (dark areas) at depths corresponding to peak values of group A (< 626 HU).

(between *c*. 82 and 68 cm). C1 and C2 show complementary trends along the sample. The proportion of C2 in the sample is high at the bottom (*c*. 50–55% between 90–83 cm) and at the top (*c*. 43–55% between 68–65 cm). The ratio of C2 ranges between 15–20% in the middle where there is a notable rise in C1. This implies that the dominant form of carbonate mineral was calcite in the middle part and dolomitic matrix in the upper and lower parts.

C1 and C2 reveal complementary trends along the sample. The percentage of the predominantly calcitic matrix (C1) is low in those parts where the proportion of calcite-filled pores (B) is minimal, i.e., the bottom and top part of the sample with values around 40–45%. Likewise, higher values of 65–75% form a plateau in the middle part of the sample (between *c*. 82 and 68 cm). This implies that calcite precipitation was relatively low in the lower and upper parts of the sample. Conversely, the dominant form of carbonate mineral was calcite in the middle part. This is further corroborated by the contrasting trends of C2 corresponding to the predominantly dolomitic matrix. The proportion of C2 in the sample is high at the bottom (*c*. 50–55% between 90–83 cm) and at the top of the sample (*c*. 43–55% between 68–65 cm). Conversely, the ratio of C2 ranges between 15–20% in the middle where there is a notable rise in C1. Conditions thus may have favoured the formation of high-magnesium calcite and dolomite in periods when the lowermost and uppermost part of the sample were laid down. Conversely, the precipitation of calcite must have prevailed in the period represented by the middle part of the sample.

The proportion of the densest component (D) corresponding to the limonite-saturated matrix is the highest in the bottom 10 cm or so of the sample (5–10%) showing a steady drop to near zero values in the upper 15 cm. The proportion of Fe and Mn is likewise high in this part (Fig. 8). This apparently means that this part was significantly influenced by large-scale fluctuations of the groundwater table in relatively drier periods. Probably bacterial activity in the lake can affect Fe and Mn, but the primary source is dissolution from bedrock loess by oxidisation of groundwater.

4.2. Member Cs-3

Two adjacent samples (II, III) were taken from Member Cs-3; sample II is here considered to be representative of this member. The graphs (Fig. 6) depict the vertical variation of identified RFCs for sample II (Member Cs-3) between depths of 65–60 cm. While empty pores appear to be missing in the lowermost two centimetres or so of the sample there is a gradual increase in the topmost 2 centimetres, reaching a maximum value of 8% at the top. These values are significantly higher than

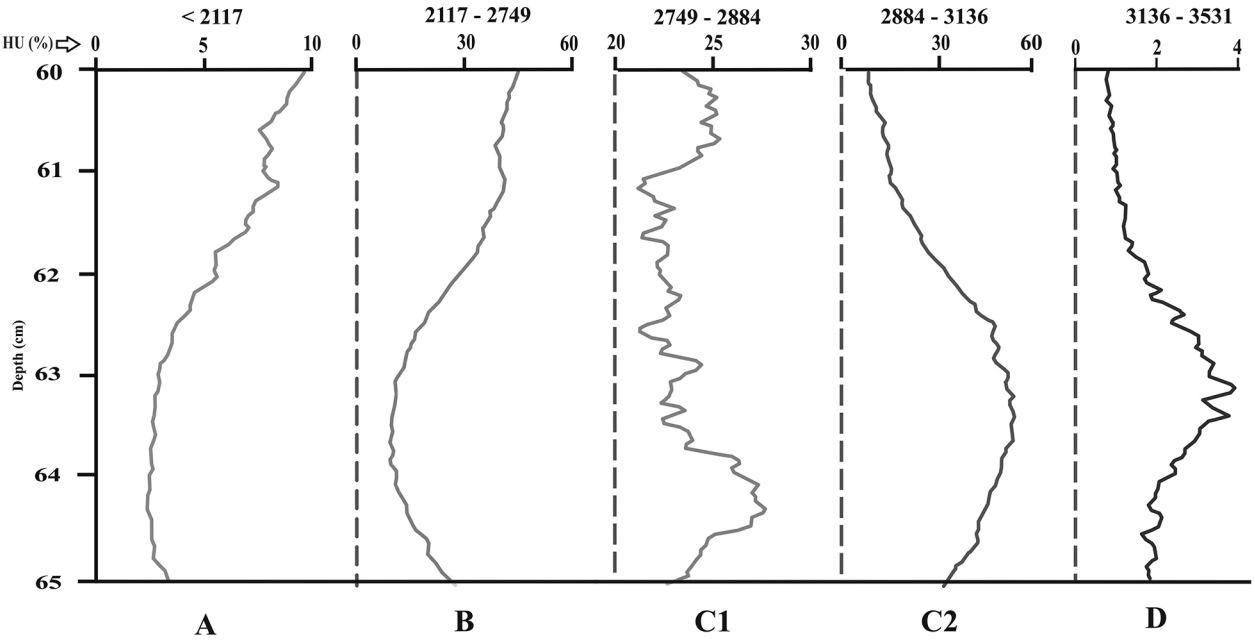

Fig. 6. Vertical changes in the proportion of identified rock-forming components (RFC) for member Cs-3. A – empty pores, B – partially filled pores, C1 – low-density, predominantly calcitic matrix, C2 – high-density, predominantly dolomitic matrix, D – highest-density, limonite-saturated dolomitic matrix. Note numbers at the top mark the HU intervals of the corresponding RFCs.

in the case of sample I, where the proportion of empty pores was below 1.6–2%. A similar trend is notable in percentage changes of group B corresponding to partially calcite-filled pores. Again, the proportions are significantly higher than in sample I, reaching values between 35–45% in the topmost two centimetres or so and close to 15–20% at the bottom. An opposing trend is notable in the proportions of C2 and D, representing high-density, predominantly dolomitic and highest density limonite saturated matrix. Here the largest proportions are confined to the lowermost three centimetres or so of the sample with values between 34–56% for group C2 and 1–4% for group D. The percentage of lower density calcitic matrix (C1) is significantly lower than that of the higher density matrix components (C2, D), with peak values of 27 and 25% in the lowermost and highest centimetre or so of the sample. It stays relatively constant for most of the sample. According to these observations, conditions favoured the formation of higher-density carbonates with a predominantly dolomitic matrix for the period captured by most of the sample (3.5 cm out of 5-cm-interval). A notable decrease in these high-density components, with a parallel increase in the lower-density matrix as well as empty pores and calcite-filled pores, is restricted to the uppermost centimetre or so, marking the emergence of highly different conditions.

4.3. Member Cs-4

Contrary to the previous sample, the carbonate of sample IV is non-lithified, although it has a similar length of *c.* 30 cm to sample I (Fig. 7). The proportion of empty pores (A) is minimal (0–1%) in the lowermost and topmost 5 cm of the sample (Fig. 7). Values are generally low between 50 and 30 cm close to 1% with several random peaks turning up at depths of 48.2, 44.5, 41.2 and 35.6 cm. However, in contrast to sample I where these peaks are sharp, here there is a gradual increase followed by a slow decrease around the mentioned peaks, which hints at the presence of not only a large number of pores but most likely a predominance of larger pores as well. In contrast to the vertical trend characterising group A, the proportion of partially filled pores remains much lower and relatively constant (1–1.5%). The proportion of the lower-density calcite-bearing matrix remains low throughout the sample (10–16%) and has a similar upward-decreasing trend. The highest proportions are notable for the higher density, predominantly dolomitic matrix component (C2) (54–66%). It is relatively constant for most of the sample (around 60% between depths of 50–33 and 26–28 cm, respectively), implying the prevalence of similar environmental conditions for a major part of the sample. Percentages of the highest density RFC (D) remain low (16–20%) for most of the sample with a gradual, slow upward increase

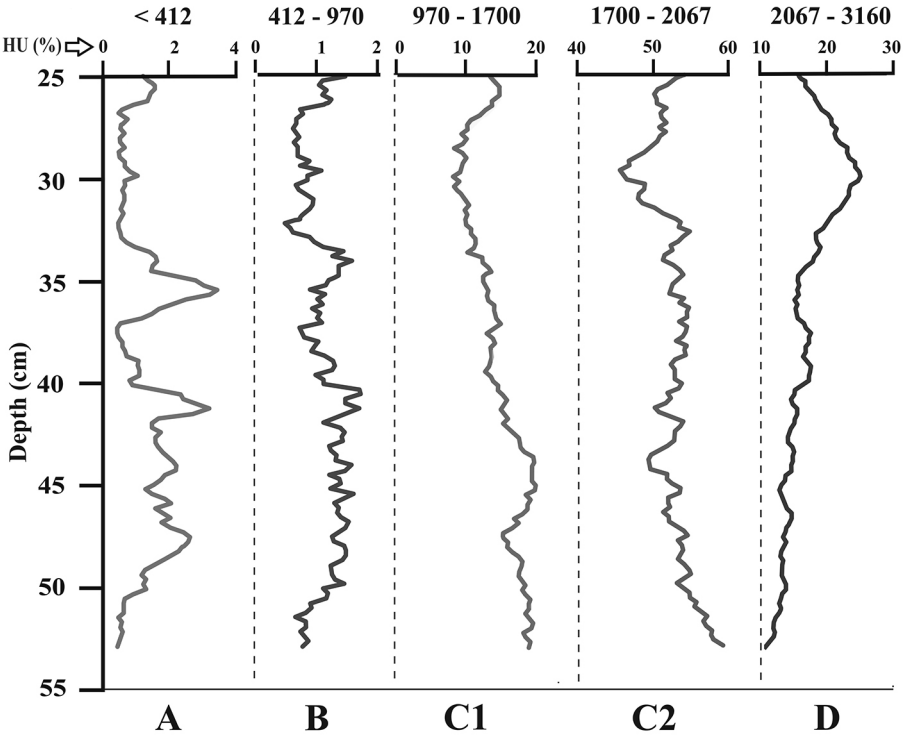

Fig. 7. Vertical changes in the proportion of identified rock-forming components (RFC) for member Cs-4. A – empty pores, B – partially filled pores, C1 – low-density, predominantly calcitic matrix, C2 – high-density, predominantly dolomitic matrix, D – highest-density, limonite-saturated dolomitic matrix. Note numbers at the top mark the HU intervals of the corresponding RFCs.

reaching peak values of 24–28% in the topmost ten centimetres or so.

5. Comparison with previously generated geochemical and palaeoecological data

As can be seen in Figure 8, at depths between 90 and 85 cm, the carbonate content is the lowest (< 10%), while the proportion of dolomite in carbonate minerals is relatively high (*c.* 30–50%). This is where the highest mean HU values are recorded, and the proportion of high-density RFCs (C2, D) is also high (Fig. 4). Ca has its all-time low as well as Sr, along with positive $d^{18}O$ (–4‰) and $d^{13}C$ (1‰) values. This implies the emergence of warmer, drier conditions with higher evaporation rates and restricted plant assimilation of CO_2, favouring the precipitation of high-magnesium calcite and dolomite (McConnaughey, 1991). The proportion of Fe is the highest in this part, indicating that the main controlling factor here is ground water table fluctuation and subsequent fluctuations in pH (compare Molnár & Botz, 1996). The trend in Mn and Fe follows that of HMC (C2, D) in the lowermost part of Sample I (Figs. 4, 8). In this interval, as shown in Figure 11, aquatic gastropods that tolerate a temporary water cover (e.g., *Anisus spirorbis* (Linnaeus, 1758)) are dominant, and the proportion of terrestrial, nearshore taxa (e.g., *Succinea oblonga (*Draparnaud, 1801)) is low, hinting at a relatively restricted shoreline and/or a smaller extension of the former water body.

In the next interval, between 85 and 75 cm, there is a marked decrease in the percentage of dolomite minerals to about half of the original value (25–27%) accompanied by a *c.* 30% rise in carbonate and *c.* 15% increase in Ca content (Fig. 8). The percentage of Fe also decreases, while the concentration of Mn significantly increases. This interval is also characterised by a negative shift in $d^{18}O$ and $d^{13}C$ values (to –8‰). Mean HU values also undergo a significant decrease to 2,500 from their original value of 2,700, marking the precipitation of lower-density minerals and lower input of higher-density minerals. The proportion of calcite-filled pores also reaches a peak value (Fig. 4). The negative shift in oxygen isotopes marks the emergence of a slightly cooler and more humid period. The likewise negative shift in carbon isotope values hints at greater extraction of CO_2 by algae responsible for the precipitation of carbonate, while high Mn values indicate higher bioproduction rates in the lake as algae accumulate higher proportions of Mn (Richardson et al., 1988; Vanderputten et al., 2000; Lazareth et al., 2003) in their bodies and this is released into the water after their death. The recurring occurrence of larger empty and calcite-filled pores (Fig. 4) hints at the expansion of the deep-rooted aquatic vegetation. As seen in Figure 11 the proportion of near-bank gastropods and those tolerating temporary water cover (*Anisus spirorbis* (Linnaeus, 1758)) decrease, while there is a marked increase in percentages of constant water taxa (e.g., *Pisidium obtusale* (Lamarck, 1818)) marking an expansion of the lake's surface and a deepening of the water under more humid conditions. Higher temperatures result in higher evaporation rates, higher salinity and pH which acts as a limiting factor in algal growth and primary production (Tompa et al., 2014; Molnár et al., 2019). Thus, a reduction in temperatures and increase in humidity favour the increase in algae in the pond by reducing the pH, lowering the concentration of Na, K ions and allowing calcite to precipitate, a process called whitening and yielding murky, milk-like waters (Thompson et al., 1997; Tompa et al., 2014; Molnár et al., 2019; Pósfai, 2020).

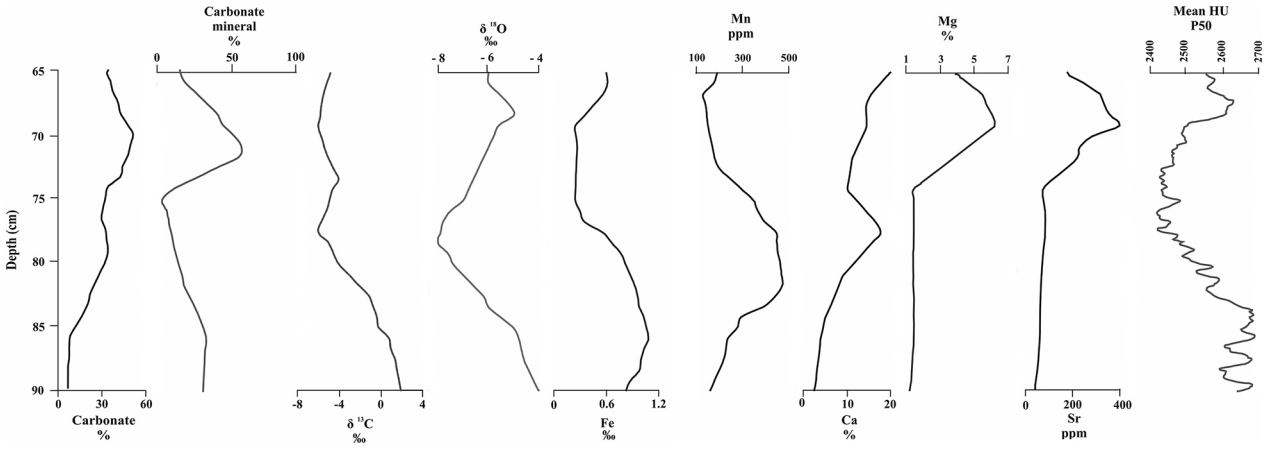

Fig. 8. Geochemical data adapted from Molnár & Botz (1996) for members Cs1 and Cs2 and mean HU values.

In the last interval, between 75 and 60 cm, there is another increase in the percentage of dolomite minerals (to 65 and 85%) accompanied by an increase in carbonate content (Fig. 8). $d^{18}O$ undergoes a positive shift (to –6‰) along with a marked increase in Sr, pointing to the emergence of more arid conditions with higher temperatures in comparison with the previous interval. Mean HU values also increase to 2,650 HU, marking the precipitation of higher-density RFCs. The highest density D component remains low (Fig. 4) just like concentrations of Fe and Mn. Thus, the appearance of a higher-density matrix is here attributable to the precipitation of high-magnesium calcite and dolomite rather than saturation by metallic components. An all-time high Mg value, as well as the high percentage of dolomite minerals (65–85%), also corroborate this assumption (Fig. 8). All in all, we can see the initial development of more arid conditions with a highly limited water coverage and significant water table and groundwater fluctuations favouring the formation of dolomitic limestone. Subsequently, cooler and more humid conditions emerge, resulting in a deepening of the lake as well as its spatial expansion along with an increase in aquatic and nearshore vegetation. In this interval, the extraction of CO_2 from the water by algae must have been the dominant control of carbonate precipitation, similar to what was seen in the interval between 85 and 75 cm (Tompa et al., 2014; Molnár et al., 2019).

In the final phase, captured by a sample I, drier conditions emerge again favouring the precipitation of high-magnesium calcite and the formation of dolomitic limestone.

In sample II (Cs-3) Fig. 9, which represents the next interval in the lake's evolution, the same trend continues at the top of sample I (Figs. 6, 8). $d^{18}O$ values remain constant and the same as in the top part of sample I (–6‰), Sr values also remain high, showing a gradual upward increase (220 to 380 ppm). All these again point to the prevalence of drier and warmer conditions favouring the precipitation of high-magnesium calcite and the formation of dolomite. The mean HU values remain above 2,600 similar to the lowermost and topmost part of sample I. In the lowermost 3 cm of sample II, this reach-

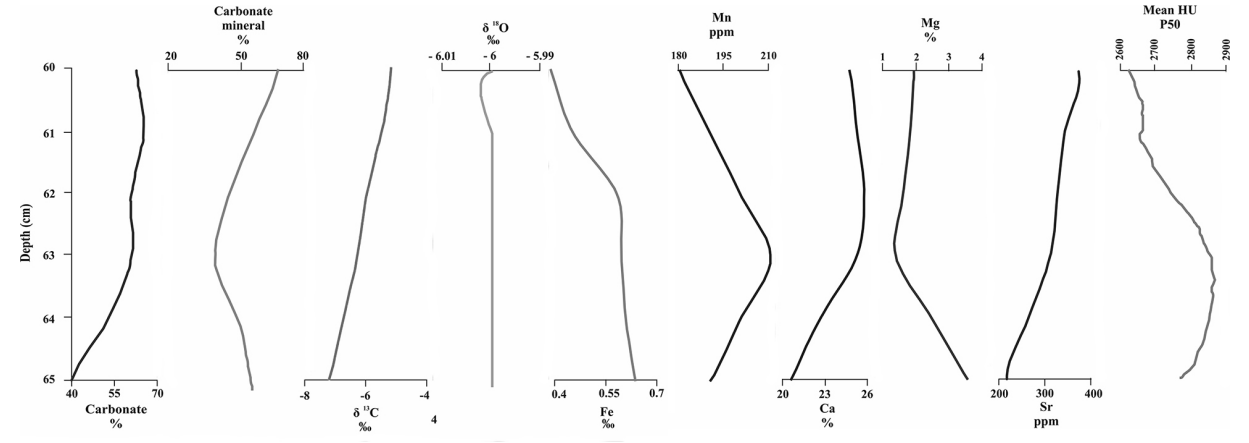

Fig. 9. Geochemical data adapted from Molnár & Botz (1996) for member Cs3 and mean HU values.

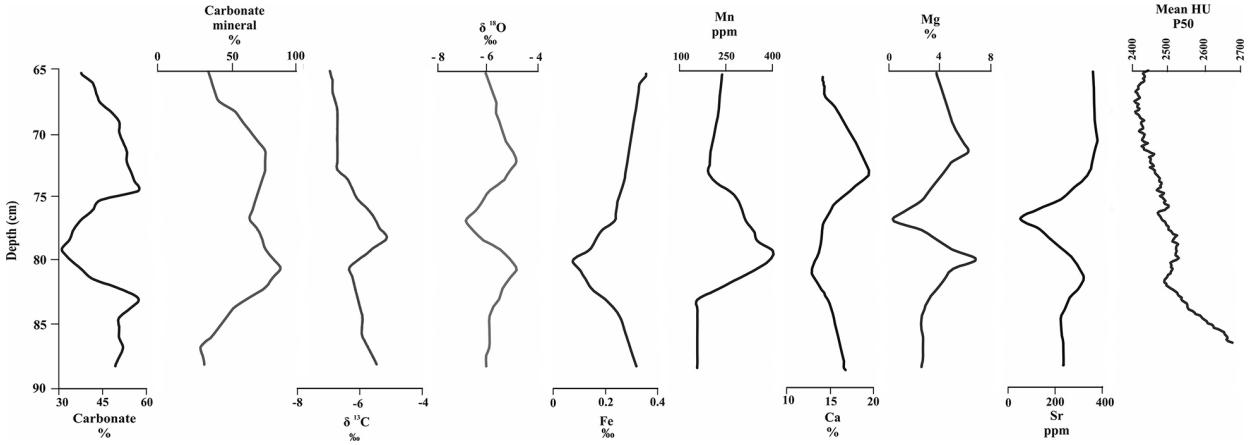

Fig. 10. Geochemical data adapted from Molnár & Botz (1996) for member Cs4 and mean HU values.

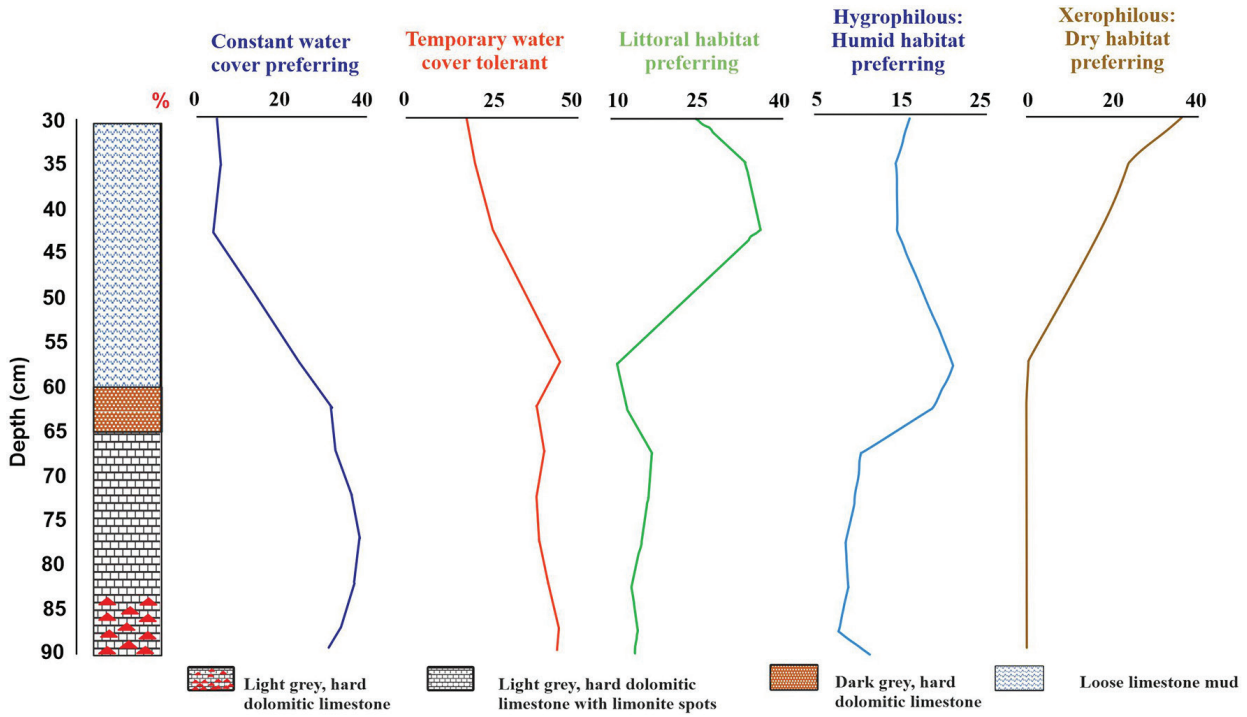

Fig. 11. Palaeoecological data for the entire section, adapted from Mucsi (1963).

es even 2,900 HU, hallmarking the predominance of higher-density minerals in the carbonate (Fig. 9). The proportions of dolomite minerals remain close to 50%, marking relatively stable conditions. The carbonate content also remains stable after an initial rise to 60%. In this part the percentage of terrestrial gastropod taxa that prefer humid habitats (*Punctum pygmea* (Draparnaud, 1801)) further increases with a continuing decrease of constant water taxa (*Pisidium obtusale* (Lamarck, 1818)), marking a drop in the water level and a reduction in the pond surface (Fig. 11).

In the topmost sample IV all geochemical parameters remain relatively constant, with the exception of the interval between 48 and 38 cm (Fig. 10). d^{18}O values remain around –6‰, the same as in the previous sample, apart from a negative shift to –7‰ in the 10-cm-interval mentioned. Sr also remains high (around and above 300 ppm) with Fe, Mg, and Ca as well as the carbonate and dolomite mineral content. Here the percentage of aquatic taxa (*Pisidium obtusale* (Lamarck, 1818)) significantly decreases, reaching their minimum in the section studied (Fig. 11). Among aquatic taxa those tolerating temporary water (*Anisus spirorbis* (Linnaeus, 1758)) prevail. Percentages of near-bank and dry habitats preferring taxa (*Chondrula tridens* (Müller, 1774)) increased significantly, marking the expansion of terrestrial habitats, a significant reduction in the lake surface and a major drop in the water level. After the initial drop mean HU values remain constant. Comparison of absolute values with those of previous samples is not possible as here the lower values hint at the lack of cementation. So again, dry conditions favoured the precipitation of high-magnesium calcite and dolomite in this part. In the mentioned 10-cm-interval between 48 and 38 cm, where a short period of cooler and more humid conditions can be presumed, a slight increase in the percentages of C1 (low-density, predominantly calcitic matrix) is also notable parallel with a slight decrease in the proportion of the higher-density C2 component (Fig. 7).

6. Comparison with extra-regional palaeohydrological and palaeoclimatological proxies from the North Atlantic and west-central Europe

Based on the developed age depth model, the first two studied samples span the interval between 10.8 and 8.8 kyr cal BP (Fig. 12). Sedimentation times varied between 33 and 80 years/cm. At the base of the section, corresponding to the interval between 10.8 and 10.4 kyr, sedimentation times were low (60–65 years/cm). This period is characterised by relatively higher mean HU val-

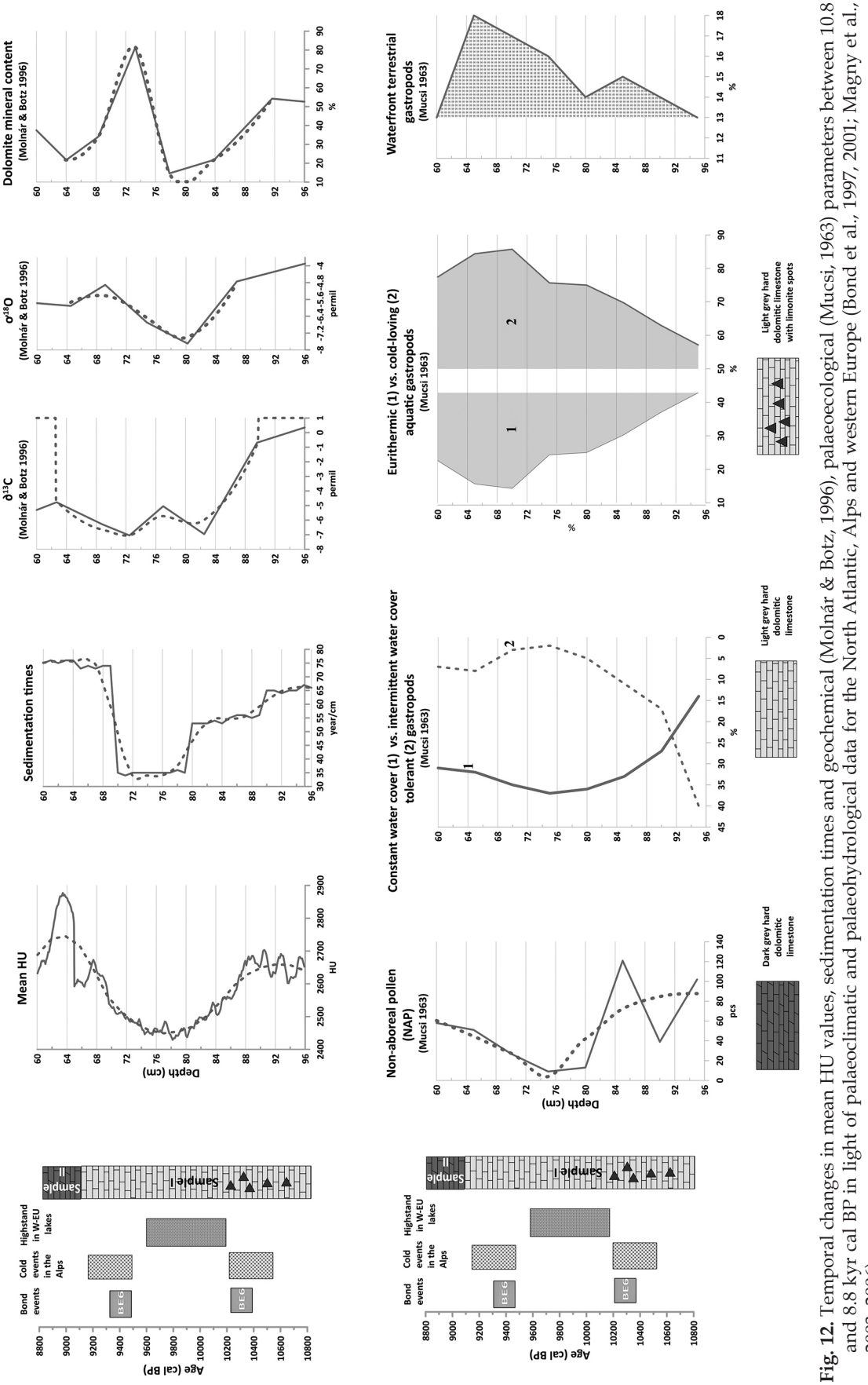

Fig. 12. Temporal changes in mean HU values, sedimentation times and geochemical (Molnár & Botz, 1996), palaeoecological (Mucsi, 1963) parameters between 10.8 and 8.8 kyr cal BP in light of palaeoclimatic and palaeohydrological data for the North Atlantic, Alps and western Europe (Bond et al., 1997, 2001; Magny et al., 2003, 2006).

ues (2,600–2,700 HU). Here both the $\delta^{13}C$ and $\delta^{18}O$ values are positive (–1 to 0 ‰ and –4.8 to –4‰, respectively), and the estimated dolomite mineral content is also high (~ 50%). The proportion of intermittent water-cover-tolerant gastropods (e.g., *Anisus spirorbis* (Linnaeus, 1758)) is likewise high (40–25%), while that of constant water-preferring taxa is low at 15–20% (*Pisidium obtusale* (Lamarck, 1818)). The amount of non-arboreal pollen grains (NAP) is also relatively high (Fig. 12). All this confirms our view of relatively warmer conditions and a greater aridity at the site. In the following period, *c.* 1 kyr to 9.4 kyr cal BP sedimentation times decreased to 30–35 years/cm, marking an increase in carbonate formation. This period is characterised by a strong negative shift in the $\delta^{13}C$ and $\delta^{18}O$ values (ca. –7 and –3‰), hallmarking the emergence of cooler and more humid conditions and greater primary production. A similar negative shift is notable in the mean HU values, indicating the precipitation of dominantly calcite. A marked decrease in the number of non-arboreal pollen NAP grains (Gramineae) also signals a reduction of open steppe areas around the lake. The water level probably rose. This is seen also in the marked decrease in intermittent water-cover-tolerant aquatic gastropods (*Anisus spirorbis* (Linnaeus, 1758)) and a major increase in the constant water-cover-preferring elements (*Pisidium obtusale* (Lamarck, 1818)). Aquatic gastropods that prefer milder conditions also significantly decrease, parallel to an increase in the proportion of cold-loving elements signalling the emergence of cooler conditions. This period is bounded by two major important climate change events: an expansion of colder conditions in the Alps (Magny et al., 2003, 2006) and a southward displacement of ice-rafted debris and cooler ocean water in the North Atlantic, referred to as Bond event 7 at 10.3 kyr cal BP and Bond event 6 at 9.4 kyr cal BP (Bond et al., 1997, 2001). As a probable result, significant cooling and increase in precipitation are notable in western Europe also seen in the high lake water levels of the Swiss Alps (Magny et al., 2003, 2006). This could have resulted in higher floodwaters on the catchment of the Danube River, yielding a higher input of freshwater to the ponds of the Danube-Tisza Interfluve through rainfall and higher groundwater tables. A reduction in temperatures also led to reduced aridity and expansion of arboreal vegetation (bushes). In the last 600 years, after *c.* 9400, conditions slowly improved leading to slightly warmer temperatures; a reduction in the water table was also seen in the expansion of waterfront terrestrial gastropod taxa (*Chondrula tridens* (Müller, 1774)) and a positive shift in all isotope and mean HU values, again hinting at the prevalence of high-magnesium calcite and dolomite precipitation.

7. Concluding remarks

Sedimentary rocks are the best archives to record past palaeoenvironmental and palaeoclimatological changes. Comparison of high-resolution biotic and abiotic proxy records enables us to reconstruct these changes at the millennial and even centennial scale, depending on the resolution attainable via sampling. Rock-forming components record information on the environmental conditions in which they are formed. In lacustrine freshwater carbonates the matrix, composed of autochthonous carbonate minerals precipitated from the water, plus additional allochthonous components (quartz, feldspars, clay minerals), yields information on sediment formation which reflects properties and changes in the sedimentary environment. To assess these changes quantitative information on the composition and proportion of rock forming components (RFCs) at high resolution is needed. The CT is sensitive to changes in density; therefore, changes in any biogeochemical parameters in the environment show changes in CT mean values. X-ray computer tomography has helped us gain quantitative data based on density differences of RFCs expressed by the Hounsfield unit values. In the present study, we have tested the applicability of the method to reveal small-scale (mm) vertical proportional variations in RFCs recording temporal sedimentary environmental changes and find correspondence with palaeoclimatic and palaeohydrological changes inferred from results of geochemical and palaeoecological investigations. Due to their lower resolution of mm-scale compared to that of micro-CT offering resolutions at the nanometre scale, data and images from medical CT are unable to tell apart micrite and sparite in carbonates, whose size is below the voxel size. Based on density differences the relative components of the matrix (autochthonous – calcite and dolomite as well as allochthonous – quartz, feldspar, clay, pellets) as a whole, the cement and pores can safely be decomposed from medical CT data. Micritic and sparitic components, as well as single particle grains, are recorded only on micro-CTs that offer higher resolution. This may be a limiting factor in the application of medical CT. However, upscaling of data from the level of micro-CT to that of medical CT is still not solved in earth sciences. Nevertheless, general density changes in the matrix captured via medical CT carries information on

sediment formation which reflects properties and changes in the sedimentary environment. Molluscan ecology, isotope geochemistry, sedimentation times and CT-based rock density changes show a strong correspondence implying that millennial-scale climatic oscillations are clearly recorded in carbonate formations of Holocene alkaline ponds of the Danube-Tisza Interfluve in southern Hungary. Seasonal temperature change affects directly the rate of evaporation which increases with a rise in temperature, increasing salt concentration and pH in the lake water. This generally leads to precipitation of high-magnesium calcite which turns into protodolomite, dolomite syngenetically in the alkaline ponds. Rocks composed of such carbonate minerals are characterised by higher densities, as reflected in positive shifts of mean HU values. In periods of lower evaporation, higher humidity, and rainfall the photosynthetic activity of algae is the predominant controlling factor in carbonate formation, resulting in the precipitation of dominantly calcite rather than high-magnesium calcite characterised by lower densities and as such lower mean HU values. Thus, application of the CT method and complex statistical analysis of the data gained seem to be suitable for revealing small-scale (millennial, centennial) sedimentary cycles recording past palaeoenvironmental changes.

Acknowledgements

Research has been carried out within the framework of the University of Szeged, Interdisciplinary Excellence Centre, Institute of Geography and Earth Sciences, and Long Environmental Changes Research Team. Support of the Ministry of Human Capacities Hungary Grants 20391-3/2018/FEKUSTRAT and NKFIH 129265 are acknowledged. The manuscript was considerably improved by valuable comments from anonymous reviewers.

References

Akaike, H., 1974. A new look at statistical model identification. *Institute of Electrical and Electronics Engineers IEEE* 19/6, 716–723.

Alzoubi, N., Geiger, J. & Gulyas, S., 2022. Defining rock-forming components of Holocene freshwater carbonates via univariate statistical and mixture analysis of CT data. *Studia Quaternaria* 39, 113–128.

Bender, M.L., Lorens, R.B. & Williams, D.F., 1975. Sodium, magnesium, and strontium in the tests of planktonic foraminifera. *Micropalaeontology* 21, 448–459.

Bhattacharyya, K., 2016. Godfrey Newbold Hounsfield (1919–2004): The man who revolutionized neuroimaging. *Annals of Indian Academy of Neurology* 19, 448–50.

Blaauw, M., Christen, J.A., Benett, K.D. & Reimer, P.J., 2018. Double the dates and go for Bayes-Impacts of model choice, dating density, and quality of chronologies. *Quaternary Science Reviews* 188, 58–66.

Bond, G., Showers, W., Cheseby, M., Lotti, R., Almasi, P., deMenocal, P., Priore P., Cullen, H., Hajdas, I. & Bonani, G., 1997. A pervasive millennial-scale cycle in North Atlantic Holocene and glacial climates. *Science* 278, 1257–1266.

Bond, G., Kromer, B., Beer, J., Muscheler, R., Evans, M.N., Showers, W., Hoffmann, S., Lotti-Bond, R., Hajdas, I. & Bonani, G., 2001. Persistent solar influence on North Atlantic climate during the Holocene. Science 294, 2130–2136.

Chen, Y., Shen, A., Pan, L., Zhang, J. & Wang, X., 2017. Features, origin, and distribution of microbial dolomite reservoirs: a case study of 4th member of Sinian Dengying Formation in Sichuan Basin, SW China. *Petroleum Exploration and Development* 44, 745–757.

Cnudde, V., Masschaele, B., Dierick, M., Vlassenbroeck, J., Van Hoorebeke, L. & Jacobes, P., 2006. Recent progress in X-ray ct as a geosciences tool. *Applied Geochemistry* 21, 826–832.

Dempster, A.P., Laird, N.M. & Rubin, D.B., 1977. Maximum likelihood from incomplete data via the EM algorithm. *Journal of Royal Statistical Society* 39, 1–38.

Duliu, O.G., 1999. Computer axial tomography in geosciences: An overview. *Earth Science Reviews* 48, 265–81.

Fang, Y. & Xu, H., 2019. A new approach to quantify the ordering state of protodolomite using XRD, TEM, and Z-contrast imaging. *Journal of Sedimentary Research* 89, 537–551.

Fourar, M., Konan, G., Fichen, C., Rosenberg, E., Egermann, P., Lenormand, R., 2005. *Tracer tests for various carbonate cores using X-Ray CT*. International Symposium of the Society of Core Analysts, Toronto, Canada, SCA2005-56.

Földes, T., Árgyelán, G.B., Kiss, B., Repa, I. & Bogner, P., 2004. Application of medical computer tomography measurements to 3D reservoir characterization. *Acta Geologica Hungarica* 47, 63–73.

Gaines, A.M., 1977. Protodolomite redefined. *Journal of Sedimentary Petrology* 47, 543–546.

Hammer, Ø., Harper, D.A.T. & Ryan, P.D., 2001. PAST: Palaeontological statistics software package for education and data analysis. *Palaeontologia Electronica* 4, 1–9.

Hicks, P.J., Ram Narayanan, K. & Deans, H.A., 1994. An experimental study of miscible displacements in heterogeneous carbonate cores using X-ray CT. *SPE Formation Evaluation,* 55–60.

Jenei, M., Gulyás, S., Sümegi, P. & Molnár, M., 2007. Holocene lacustrine carbonate formation: old ideas in the light of new radiocarbon data from a single site in central Hungary. *Radiocarbon* 49, 1017–1021.

Kenter, J.A.M., 1989. Applications of computerized tomography in sedimentology. *Marine Geotechnology* 8, 201–211.

Ketcham, R.A. & Carlson, W.D., 2001. Acquisition, optimization, and interpretation of X-ray computed tomographic imagery: Applications to the geosciences. *Computers and Geosciences* 27, 381–400.

Kercsmár, Z., 2015. *Surface geology of Hungary. Geological study*. Geological and Geophysical Institute of Hungary, 66 pp.

Lazareth, C.E, Vanderputten, E., André, L. & Dehairs, F., 2003. High-resolution trace element profiles in shells of the mangrove bivalve Isognomon ephippium: a record of environmental spatiotemporal variations. *Estuarine, Coastal and Shelf Science* 57, 1103–1114.

Magny, M., Bégeot, C., Guiot J. & Peyron, O., 2003. Contrasting patterns of hydrological changes in Europe in response to Holocene climate cooling phases. *Quaternary Science Reviews* 22, 1589–1596.

Magny, M., Leuzinger, U., Bortenschlager, S. & Haas, J.N., 2006. Tripartite climate reversal in Central Europe 5600–5300 years ago. *Quaternary Research* 65, 3–19.

Markussen, Ø., Dypvik, H., Hammer, E., Long, H. & Hammer, Ø., 2019. 3D characterization of porosity and authigenic cementation in Triassic conglomerates/arenites in the Edvard Grieg field using 3D micro-CT imaging. *Marine and Petroleum Geology* 99, 265–281.

Maurício, A., Pereira, M.F., Rocha, C., Figueiredo, C. & Marques, J.M., 2017. X-ray micro-CT study of Cabeço De Vide serpentinites and carbonate rock samples: a preliminary approach. *Procedia Earth and Planetary Science* 17, 952–955.

Mcconnaughey, T., 1991. Calcification in Chara Corallina: CO2 hydroxylation generates protons for bicarbonate assimilation. *Limnology and Oceanography* 36, 619–28.

Miháltz, I., 1947. *A Duna-Tisza csatorna geológiai viszonyainak tanulmányozása – A Duna-Tisza csatorna* [*Study of the geological conditions of the Danube-Tisza channel*]. A Magyar Földmívelésügyi Minisztérium kiadványa, Budapest, pp. 3–12 (in Hungarian).

Miháltz, I., 1953. *A Duna-Tisza köze déli részének földtani felvétele – MÁFI évi jelentése az 1950 évről* [*Geological survey of the southern part of the Danube-Tisza junction – MÁFI annual report for the year 1950*], pp. 113–148.

Miháltz, I. & Faragó, M., 1946. *A Duna-Tisza közi édesvízi mészkőképződmények* [*Freshwater limestone formations between the Danube and Tisza*]. *Az Aéfölf Tudományos Intézet 1944–45. évi Évkönyve* 1. Szeged, pp. 371–384 (in Hungarian).

Molnár, B., 1970. On the origin and hydrogeology of natron lakes in the southern Great Hugarian Plain. *Móra Ferenc Múzeum Évkönyve* 1, 65–76.

Molnár, B., 1976. Recent lacustrine dolomite formation in The Great Hungarian Plain. *Acta Geologica Academai Scientiarum Hungaricae* 20, 179–198.

Molnar, B., 1980. Diagenetic and lithification processes of recent hypersaline dolomites on the danube-tisza interfluve. *Mineralogical Magazine* 24, 315–37.

Molnár, B., 1988. Quaternary geohistory of the Hungarian part of the Danube-Tisza Interfluve. *Proceedings of Geo Institute* 21, 61–78, Belgrade.

Molnár, B., 1991. *Modern lacustrine calcite, dolomite, and magnesite formation in Hungary*. Department of Quaternary Geology, University of Turku, 1–22 pp.

Molnár, B. & Botz, R., 1996. Geochemistry and stable isotope ratio of modern carbonate in natron lakes of the Danube-Tisza Interfluve, Hungary. *Acta Geologica Hungarica* 39, 153–174.

Molnár, B. & Szónoky, M., 1976. *On the origin and geohistorical evolution of the natron lakes of the Bugac Region*. Móra F. Múzeum Évkönyve, Szeged 1974/75, 257–270.

Molnár, B., Hum, L. & Fényes, J., 1995. Investigation of modern geological processes in Holocene lacustrine carbonates in the Danube-Tisza Interfluve – Hungary. *Acta mineralogica-petrographica*, Szeged, 36, 73–87.

Molnár, B., Murvai, M.I. & Hegyi-Pakó, J., 1976. Recent lacustrine dolomite formation in The Great Hungarian Plain. *Acta Geologica Academai Scientiarum Hungaricae* 20, 179–198.

Molnár, S., Bakacsi. Z., Balog, K., Bolla, B. & Tóth, T., 2019. Evolution of a salt-affected lake under changing environmental conditions in Danube-Tisza Interfluve. *Carpathian Journal of Earth and Environmental Sciences* 14, 77–82.

Mucsi, M., 1963. Finomrétegtani visózsgálatok a kisunsági édesvizi karbonátképződményekben [Fine-stratigraphic viscosities in the Kisunság freshwater carbonate formations] *Földtani Közlöny* 93, 373–386 (in Hungarian).

Müller, G. & Wagner, F., 1978. *Holocene carbonate evolution in Lake Balaton (Hungary): a response to climate and impact of man*. IAS Special Publication 2, 57–81.

Müller, G., Irion, G. & Förstner, U., 1972. Formation and diagenesis of inorganic Ca-Mg carbonates in the lacustrine environment. *Die Naturwissenschaften* 59, 158–164.

Oliveira, G., Geia, M., Missagia, R., Neto, I., Santos, V. & Paranhos, R., 2020. Core plug and 2D/3D-image integrated analysis for improving permeability estimation based on the differences between micro- and macroporosity in Middle East carbonate rocks. *Journal of Petroleum Science and Engineering* 193, 107335.

Pósfai, M., 2020. A Balaton üledékének ásványai (Minerals in the sediments of Lake Balaton). *Földtani Közlöny* 150/4, 511–528.

Reimer, P., Austin, W., Bard, E., Bayliss, A., Blackwell, P.G., Ramsey, C., Butzin, M., Cheng, H., Edwards, R., Friedrich, M., Grootes, P., Guilderson, T., Hajdas, I., Heaton, T., Hogg, A., Hughen, K., Kromer, B., Manning, S., Muscheler, R., Palmer, J., Pearson, C., Plicht, J., Reimer, R., Richards, D., Scott, E., Southon, J., Turney, C., Wacker, L., Adolphi, F., Büntgen, U., Capano, M., Fahrni, S., Fogtmann-Schulz, A., Friedrich, R., Köhler, P., Kudsk, S., Miyake, F., Olsen, J., Reinig, F., Sakamoto, M., Sookdeo, A. & Talamo, S., 2020. The IntCal20 northern hemisphere radiocarbon age calibration curve (0–55 cal kBP). *Radiocarbon* 62, 725–757.

Richardson, L.L., Aguilar, C. & Nealson, K.H., 1988. Manganese oxidation in pH and O_2 microenvironments produced by phytoplankton. *Limnology and Oceanography* 33, 352–363.

Sümegi, P., Molnár, D., Sávai, S., Náfrádi, K., Novák, Z., Szelepcsényi, Z. & Törőcsik, T., 2015. First radiocarbon dated palaeoecological data from the freshwater carbonates of the Danube-Tisza interfluve. *Open Geosciences* 7, 40–52.

Sümegi, P. & Náfrádi, K., 2015. A radiocarbon-dated cave sequence and the Pleistocene/Holocene transition in Hungary. *Open Geosciences* 1, 783–798.

Thompson, J.B., Schultze-Lam, S., Beveridge, T.J., Des Marais, D.J., 1997. Whitening events: biogenic origin due to the photosynthetic activity of cyanobacterial picoplankton. *Limnology and Oceanography* 42/1, 133–141.

Tompa, É., Nyírő-Kósa, I., Rostási, Á., Cserny, T., Pósfai, M., 2014. Distribution and composition of Mg-calcite and dolomite in the water and sediments of Lake Balaton. *Central European Geology* 57, 113–136.

Tullner, T. & Cserny, T., 2003. New aspects of lake-level changes: Lake Balaton, Hungary. *Acta Geologica Hungarica* 46, 215–38.

Vanderputten, E., Dehairs, F., Keppens, E. & Baeyens, W., 2000. High-resolution distribution of trace elements in the calcite shell of modern Mytilus edulis: environmental and biological controls. *Geochemica et Cosmochemica Acta* 64, 997–1011.

Wilding, M., Lesher, C.E. & Shields, K., 2005. Applications of neutron computed tomography in geosciences. *Nuclear instruments and methods in physics research A*, 542, 290–295.

Manuscript submitted: 16 September 2022
Revision accepted: 10 February 2023